Combustion and Flame 159 (2012) 3007–3013

Contents lists available at SciVerse ScienceDirect

Combustion and Flame

journal homepage: www.elsevier.com/locate/combustflame

A shock tube study of the rate constants of HO_2 and CH_3 reactions

Zekai Hong [1], David Frank Davidson *, King-Yiu Lam, Ronald Kenneth Hanson

Department of Mechanical Engineering, Stanford University, Stanford, CA 94305, USA

ARTICLE INFO

Article history:
Received 2 March 2012
Received in revised form 20 April 2012
Accepted 24 April 2012
Available online 18 May 2012

Keywords:
Shock tube
Laser absorption
$CH_3 + HO_2$
Rate constant determination

ABSTRACT

HO_2 and CH_3 are major intermediate species presented during the oxidation of natural gas at intermediate temperatures and high pressures. Previous theoretical calculations have identified several product channels for HO_2 and CH_3 reactions, with $CH_3 + HO_2 \rightarrow CH_3O + OH$ and $CH_3 + HO_2 \rightarrow CH_4 + O_2$ being the dominant reaction pathways. Both reaction pathways play an important role in the kinetics of CH_4 oxidation as $CH_3 + HO_2 \rightarrow CH_3O + OH$ is a chain-branching reaction whereas $CH_3 + HO_2 \rightarrow CH_4 + O_2$ a chain termination reaction.

$H_2O_2/CH_4/Ar$ mixtures were shock-heated to a temperature between 1054 and 1249 K near 3.5 atm to initiate the reaction. OH radicals yielded from H_2O_2 thermal decomposition react with H_2O_2 and CH_4 respectively to produce HO_2 and CH_3 in the reacting system. Using laser absorption spectroscopy, time-histories of H_2O, OH and HO_2 were measured behind reflected shock waves. The rate constant of reaction $CH_3 + HO_2 \rightarrow CH_3O + OH$ was determined to be 6.8×10^{12} cm^3 mol^{-1} s^{-1} with an uncertainty factor of 1.4. The rate constant of the competing $CH_3 + HO_2 \rightarrow CH_4 + O_2$ reaction was determined to be 4.4×10^{12} cm^3 mol^{-1} s^{-1}, with an uncertainty factor of 2.1. In addition, the rate constants of two other major reactions of the reacting system, H_2O_2 (+M) → 2OH (+M) and $OH + CH_4 \rightarrow CH_3O + OH$, were found to have excellent agreement with values recommended in literature.

1. Introduction

Hydroperoxyl radicals (HO_2) and their reactions become increasingly important in methane oxidation at elevated pressures [1]. At intermediate temperatures (1000–1500 K) and high pressures (>40 atm), the dominant species in the radical pool during methane oxidization are the relatively unreactive CH_3 and HO_2. A major CH_3 oxidization pathway at these conditions [3] is via the reaction

$$CH_3 + HO_2 \rightarrow CH_3O + OH \qquad \text{(Rxn.1)}$$

Rxn. 1 is a major chain branching reaction, as highly reactive OH radicals are generated from the much less reactive CH_3 and HO_2 radicals. In addition, the resulting methoxy radicals (CH_3O) are very unstable and easily decompose to form H atoms and CH_2O. Therefore, Rxn. 1 is critical to characterizing natural gas combustion at intermediate temperatures and high pressures.

Besides Rxn. 1, other product channels are possible from the reaction of CH_3 and HO_2, and potential energy surfaces (PES) for these pathways have been proposed in previous theoretical studies [2,4]. Among all the product channels, the hydrogen abstraction reaction (on a triplet surface)

$$CH_3 + HO_2 \rightarrow CH_4 + O_2 \qquad \text{(Rxn.2)}$$

is also of particular importance to the modeling of high-pressure CH_4 oxidation. As opposed to Rxn. 1 being a chain branching reaction, Rxn. 2 is a chain termination reaction. The branching ratio of the two product channels, $CH_3O + OH$ and $CH_4 + O_2$, is important in modeling ignition in high-pressure combustion systems [2]. Furthermore, the reverse reaction of Rxn. 2 ($CH_4 + O_2 \rightarrow CH_3 + HO_2$) is regarded as a significant initiation reaction for CH_4 ignition [5]. Rxn. 2 is also possible on a singlet surface, but that reaction rate is expected to be negligible compared to that on the triplet surface [2,4].

Despite the significance for both k_1 and k_2, very little experimental data are available. Baulch et al. [6] assigned a k_1 uncertainty of an order of magnitude based on an early indirect experimental study [7]. Scire et al. [8,9] studied CO oxidation with CH_4 perturbations in a flow reactor to get estimations for both k_1 and k_2, but "some uncertainty remains due to the indirect nature of these determinations" [2]. To our knowledge, only Rxn. 2 has received an experimental investigation, and that was by Srinivasan et al. [5], where OH time-histories were measured at the onset of CH_4 oxidation to evaluate the rate constant of the reaction in its reverse direction (k_{-2}). An uncertainty of ± 50% was assigned to k_{-2} [5].

* Corresponding author.
E-mail address: dfd@stanford.edu (D.F. Davidson).
[1] Present address: Combustion Research Engineer at General Electric Company, Global Research Center, Niskayuna, NY 12309, USA.

0010-2180/$ - see front matter © 2012 The Combustion Institute. Published by Elsevier Inc. All rights reserved.
http://dx.doi.org/10.1016/j.combustflame.2012.04.009

The first attempt to predict k_1 using first-principles was performed by Zhu and Lin [4]. However, another recent theoretical study by Jasper et al. [2] found that Zhu and Lin's k_1 values are four times larger than theirs. To make the situation more complicated, k_1 values adopted in modern kinetic mechanisms [10–14] vary by as much as a factor of 5. The first theoretical prediction of k_2 was also performed in the same study of Zhu and Lin [4].

Recent advances in shock tube/laser absorption techniques now make it possible to consider new methods to measure HO_2 reaction rates. These advances include the development of a sensitive H_2O diagnostic, and application of a simpler method to generated H_2O_2, both of which were used to study H_2O_2 thermal decomposition at intermediate combustion temperatures [15–17]. These advances have yielded a substantially improved understanding of H_2O_2 and HO_2 reactions. Additionally, H_2O_2 has been proposed as an HO_2 precursor for investigating reactions between HO_2 and combustion hydrocarbon species [15]. The goal of this work is to apply these advances to the study of the reaction of CH_3 and HO_2.

2. Experiment design and setup

2.1. Test reagents and preparations

It has been demonstrated that a sizeable HO_2 radical pool can be formed during the thermal decomposition of H_2O_2 [15,16]. The majority of HO_2 is yielded through a two-step process:

$$H_2O_2(+M) \rightarrow 2OH(+M) \quad \text{(Rxn.3)}$$

$$OH + H_2O_2 \rightarrow H_2O + HO_2 \quad \text{(Rxn.4)}$$

With HO_2 radicals present at substantial concentrations during the decomposition of H_2O_2, reactions between HO_2 and CH_3 can be established with the introduction of a CH_3 radical pool.

Although a few CH_3 precursors have been identified and successfully applied previously [24], to blend very reactive H_2O_2 vapor with chemically unstable CH_3 precursors could be problematic. However, CH_4, being a very stable gaseous hydrocarbon, at standard conditions may be added to the H_2O_2 reacting system as a source of CH_3 radicals. Following Rxn. 3, OH radicals can be generated at large quantities, which subsequently undergo H-abstraction reaction with CH_4 to form CH_3 radicals:

$$OH + CH_4 \rightarrow H_2O + CH_3 \quad \text{(Rxn.5)}$$

Following Rxns. 3–5, both CH_3 and HO_2 radicals can be produced at sizeable concentrations as H_2O_2 starts to decompose in the presence of CH_4. Thus, CH_4 and H_2O_2 blends were chosen as reagents in this work to investigate the rate constants of $CH_3 + HO_2$ reactions (Rxns. 1 and 2). It should be noted that the fate of the majority of CH_3 radicals from Rxn. 5 is to recombine to form stable C_2H_6.

Test mixtures were prepared by passing a stream of 1% CH_4/99% Ar (by mole) blend through a vessel that steadily generates H_2O_2 vapor; details of the H_2O_2 generator can be found in Ref. [15]. The CH_4/Ar blend doped with H_2O_2 vapor was subsequently directed to the test section of a shock tube facility, as will be discussed in the next subsection. H_2O and O_2 may also appear in test mixtures, as a portion of H_2O_2 has already decomposed by the time an experiment can be initiated. Since the addition of $H_2O_2/H_2O/O_2$ does not change the mole ratio between CH_4 and Ar in test mixtures, the compositions of test mixture can be fully characterized once the concentrations of doped $H_2O_2/H_2O/O_2$ are measured.

2.2. Shock tube facility

Experiments were carried out in a Stanford University shock tube facility behind reflected shock waves. The shock tube has a 3.7 m driver section and a 10 m driven section, both of which have an inner diameter of 15.2 cm. Using standard normal shock relations, temperatures and pressures behind reflected shock waves can be calculated using incident shock speeds measured with a series of piezoelectric pressure transducers over the last 1.5 m of the shock tube. More specifics of the shock tube facility have been reported elsewhere [16].

2.3. Design for diagnostics

A sensitive H_2O diagnostic has proven to be essential to the improved understanding of the H_2O_2 pyrolysis system [15–17], particularly for the determination of initial H_2O_2 loadings and the rate constant of Rxn. 3. However, the one-for-one conversion between H_2O_2 and H_2O that holds for pure H_2O_2 decomposition cannot be directly adopted in the current study, because an additional major channel for H_2O production becomes available with the presence of CH_4 through Rxn. 5. Nevertheless, the overall H_2O production can be reliably linked to the initial H_2O_2 loading knowing the rate constants for Rxns. 4 and 5 (k_4 and k_5). The H_2O diagnostic also provides key information on the rate constant of Rxn. 3 (k_3).

In addition to the H_2O diagnostic, the OH diagnostic was also included, because OH time-histories may be used to infer the rate constant of our primary target reaction (Rxn. 1). The chemical equation of Rxn. 1 suggests that OH radicals are a direct product of the reaction. In addition, the other product of Rxn. 1, CH_3O, undergoes rapid decomposition to release H atoms, which in turn react with O_2 to generate OH radicals. One seeming obstacle is that reactions other than the target Rxn. 1 also influence OH time-histories, for example, Rxn. 3 as a major source of OH and Rxns. 4 and 5 major OH sinks. However, the fact that both reactants of Rxn. 1 are transient intermediate species dictates that the effects of Rxn. 1 are most pronounced only when both HO_2 and CH_3 concentrations are near their peak values. Therefore, the strong temporal localization of Rxn. 1 makes it feasible to determine the rate constant (k_1) by analyzing OH time-histories despite interfering reactions. As will become evident when the k_1 uncertainty is accessed in Section 3.3, uncertainties from the interfering reactions (Rxns. 3–5) do not combine cumulatively due to the constraints of the experimental data. Experimental uncertainty in k_1 can be further reduced by knowing the rate constants of the major interfering reactions (Rxns. 3–5) which are or can be accurately determined.

The other target of the current study, $CH_3 + HO_2 \rightarrow CH_4 + O_2$ (Rxn. 2), does not directly alter OH concentrations, and thus it is difficult to infer k_2 from OH time-histories measurements. However, both Rxns. 1 and 2 consume HO_2 radicals. It is therefore feasible to infer the combined rate constant of all product channels of the $CH_3 + HO_2$ reactions from HO_2 time-histories. Because product channels other than Rxns. 1 and 2 are negligible [2,4], information on the summations of k_1 and k_2 may be obtained by analyzing HO_2 time-histories. Given k_1 values determined from OH time-histories, determination of k_2 is then also possible.

It should be noted that although it might be also possible to infer k_2 using a CH_3 diagnostic, the HO_2 diagnostic was chosen from a spectroscopy perspective. The CH_3 absorption band in the UV near 200–225 nm [17–20] is entirely overlapped by the much broader HO_2 and H_2O_2 spectra [21–23]. At the same time, the interference from CH_3 absorption is negligible at the wavelength selected for the HO_2 diagnostic (227 nm [16]).

From the discussion above, time-histories of three species (H_2O, OH, and HO_2) need to be simultaneously measured to uniquely determine the composition of test mixtures, and the rate constants

of two target reactions (k_1 and k_2). In parallel to this work, the same combination of laser diagnostics has been successfully used to obtain a comprehensive understanding of the H_2O_2 thermal decomposition system [16]. A detailed description of the diagnostic setup for measuring the time-histories of all three species can be found in the same study [16] and is not elaborated here.

3. Results and discussion

3.1. Initial composition of test mixtures

Shown in Fig. 1 is a sample H_2O time-history (upper panel) and the corresponding H_2O sensitivity analysis (bottom panel); the test was performed at 1103 K, 3.56 atm. Before any kinetic data can be obtained, the composition of test mixtures needs to be determined. During the decomposition of neat H_2O_2 [15], all the hydrogen content in the resulting H_2O is from the sole reactant H_2O_2, dominantly through Rxn. 4 ($OH + H_2O_2 \rightarrow HO_2 + H_2O$). In the presence of CH_4, a considerable amount of additional H_2O is formed through Rxn. 5 ($OH + CH_4 \rightarrow CH_3 + H_2O$) following H_2O_2 decomposition. From a hydrogen balance perspective, Rxn. 5 is a channel that supplies the H_2O_2 decomposition system with extra hydrogen content from CH_4. As Rxns. 4 and 5 compete for OH radicals, a larger k_5 has the similar effect as a smaller k_4 in promoting final H_2O yields, which is confirmed by the H_2O sensitivity when the plateau in H_2O concentration is approached (between 1.5 and 3 ms in Fig. 1).

Although the one-for-one conversion between H_2O_2 and H_2O [15] does not hold with the addition of CH_4, it is still feasible to infer the initial H_2O_2 loading from the final H_2O yield as the uncertainty in k_4 and k_5 can be minimized. Specifically, k_4 has been measured within an uncertainty of ±13% in the temperature range of the current study [15], whereas k_5 can be determined with an accuracy of ±15% from the OH time-history of the same experiment, as will be discussed later in this section. Furthermore, the fact that the H_2O plateau level is not a strong function of k_4 and k_5 ensures that the determination of the initial H_2O_2 loading is relatively immune to small uncertainties in k_4 and k_5. At the same time, the target reactions (k_1 and k_2) have negligible sensitivities to the final H_2O yield. Therefore, the final H_2O yield is predominantly controlled by the initial H_2O_2 loading.

For the example H_2O profile shown in Fig. 1, the initial and final H_2O concentrations were measured to be 820 and 3010 ppm, respectively. An initial H_2O_2 loading of 1240 ppm was determined to account for the total H_2O yield of 2190 ppm. O_2 concentration in the initial test mixture was estimated to be 410 ppm, half of the initial H_2O value, because both O_2 and H_2O were the products of spontaneous H_2O_2 decomposition prior the reflected shock wave experiment. The $H_2O_2/H_2O/O_2$ doping only accounts for a very small portion of the test mixture; the remaining majority consists of the 1:99 CH_4–Ar blend (by mole). Therefore, the composition of the test mixture was determined to be 820 ppm H_2O/1240 ppm H_2O_2/410 ppm O_2/9975 ppm CH_4/balance Ar. It should be noted that kinetic modeling suggests that the initial O_2 concentration does not affect the H_2O yield.

Both the best-fit H_2O profile and H_2O sensitivity plot were generated using an updated version of USC-Mech II [13], a recent detailed chemical kinetic mechanism for H_2/CO/C1–C4 compounds, and the Senkin [25] kinetics code. The definition of the sensitivity coefficient is given in Ref. [26]. The updates to USC-Mech II include the latest data for the rate constants for the C_2H_6 decomposition [24], the reactions $H + O_2 \rightarrow OH + O$ [26], $OH + HO_2 \rightarrow H_2O + O_2$ [17], $HO_2 + HO_2 \rightarrow H_2O_2 + O_2$ [17], and $OH + H_2O_2 \rightarrow H_2O + HO_2$ [16]. The rate constants of two reactions that are critical to the determination of k_1 and k_2, H_2O_2 (+M) → 2OH (+M), and $CH_4 + OH \rightarrow CH_3 + H_2O$ need to be evaluated/confirmed from each set of experimental data and updated to the base mechanism, as will be discussed in the next subsection.

3.2. Determination of k_3 and k_5

As can be seen from the H_2O sensitivity analysis (Fig. 1) and the corresponding one for OH (Fig. 2), Rxns. 3–5 play major roles in the decomposition of H_2O_2 decomposition in CH_4–Ar bath gases and need to be determined with high accuracies. Among the three key rate constants, k_4 is known within an experimental error of ±13% [15] at the temperatures of the current study and was not further investigated. In contrast to k_4, the uncertainty in k_3 was estimated to be ±23% [16], with the uncertainty in temperature being the major source of error. It has been demonstrated that the temperature uncertainty in k_3 can be insulated from the rest of the reacting system by evaluating k_3 for each individual test from the corresponding H_2O time-history [15]. In addition, k_5 is only known with a factor-of-two uncertainty [6]. It is therefore a prerequisite to accurately determine k_3 and k_5 for each test to reduce uncertainties in k_1 and k_2.

As illustrated in the H_2O sensitivity plot in Fig. 1, the H_2O profile is predominantly controlled by the H_2O_2 decomposition reaction; and thus k_3 can be evaluated by matching H_2O time-histories. For the example case shown in Fig. 1, the measured H_2O profile

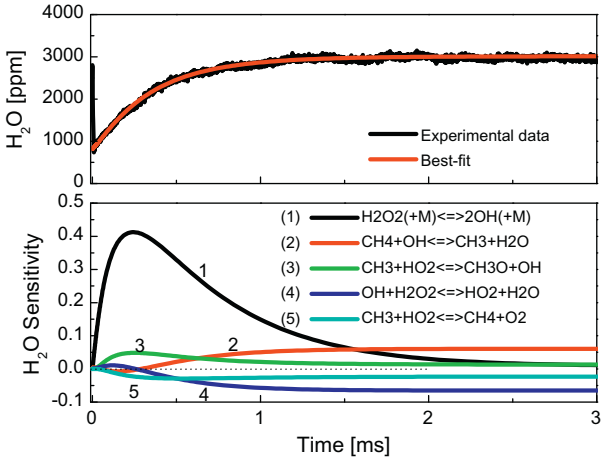

Fig. 1. (upper): example H_2O time-history; (lower): the corresponding H_2O sensitivity plot. Test mixture consists of 820 ppm H_2O, 1240 ppm H_2O_2, 410 ppm O_2, 9975 ppm CH_4, and balance Ar. The experiment was conducted at 1103 K and 3.56 atm. k_3 was determined to be 4.2×10^7 cm^3 mol^{-1} s^{-1}.

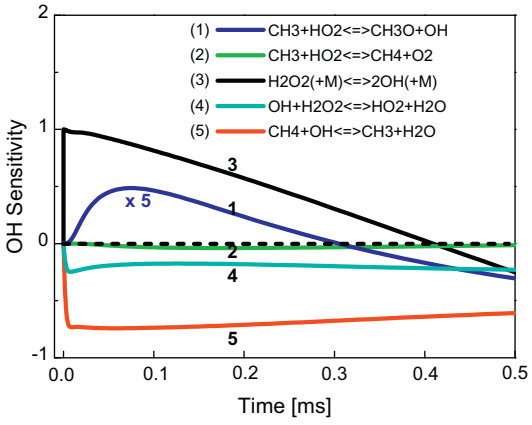

Fig. 2. OH sensitivity plot at the conditions of Fig. 1. Note that the sensitivity coefficient of reaction $CH_3 + HO_2 \rightarrow CH_3O + OH$ has been multiplied by 5.

can be best-fitted with a k_3 value of 4.2×10^7 cm^3 mol^{-1} s^{-1}. It should be noted that all the sensitivity analyses and best-fit plots reported in this article were calculated using final assessed rate constants for Rxns. 1–5. A ± 10% uncertainty in k_3 is associated with the procedure of fitting the H_2O profile, which is evaluated to be the largest source of error for k_3. In addition, uncertainties in k_1, k_2, k_4, and k_5 can propagate to k_3; the combined uncertainty in k_3 (excluding temperature uncertainty) was estimated to be ±14%.

While k_3 is mainly determined from H_2O time-histories, k_5 can be inferred from OH time-histories. Immediately following the initial jump in OH concentration, a quasi-steady state in OH concentration is reached, where the concentrations of secondary species, such as HO_2, CH_3 and C_2H_6, are negligibly small. Therefore, the initial OH concentration is predominantly controlled by the equilibrium between one OH production channel (Rxn. 3) and two OH consumption channels (Rxns. 4 and 5), which can be represented by the following expression:

$$K_3[H_2O_2] = k_4[OH][H_2O_2] + k_5[OH][CH_4]$$

where H_2O_2 and CH_4 concentrations were essentially unchanged from their initial concentrations when the OH quasi-steady state was first established.

In the example case, the height of the initial OH jump was measured to be 4.7 ± 0.1 ppm, as shown in Fig. 3. Using the expression presented in the previous paragraph and the initial mixture's composition inferred from the H_2O diagnostic, k_5 was determined to be 1.7×10^{12} cm^3 mol^{-1} s^{-1}. An analysis of uncertainty propagation suggests that for the example case k_5 has an uncertainty of ±19%, with k_3 uncertainty as the major source of error. Although the nominal level of k_5 uncertainty is notable, it should be pointed out that in order to match the concentration of the initial OH jump, k_3 and k_5 are to be used in pairs, as it is the case with all subsequent analyses. For a given k_3, the uncertainty in k_5 is negligible (approximately ±5%).

3.3. Evaluation of k_1

A careful examination of the sample OH time-history (Fig. 3) reveals that OH concentration rises gradually after the initial jump. Recall that OH decay during the decomposition of neat H_2O_2 was monotonic [15] after the initial jumps, because H_2O_2 as the sole OH source is being consumed and no other channels can replenish OH. However, with the presence of CH_4, OH can be regenerated through Rxn. 1, both directly and indirectly (see discussion in Section 2.3). Note that CH_3 and HO_2 are formed by consuming equal amounts of OH. With the new OH formation channel established by Rxn. 1 and subsequent steps, accumulating CH_3 and HO_2 act as buffers for OH. This added reaction pathway also explains the gradual rise in OH after the initial jump. The goal of this subsection is to quantitatively determine k_1 from OH time-histories.

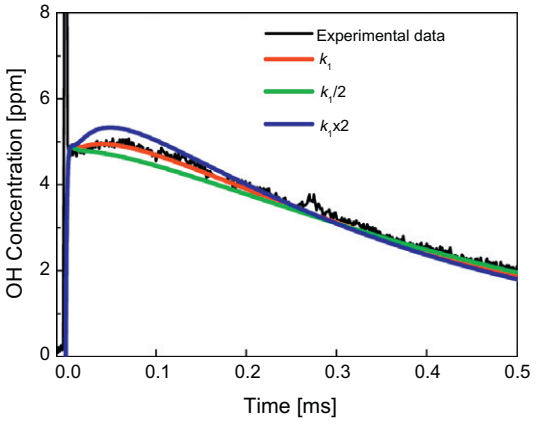

Fig. 3. A best-fit to the experimental OH time-history yields a k_1 value 5×10^{12} cm^3 mol^{-1} s^{-1}. For comparison, calculated OH profiles using non-optimal k_1 values are presented in the plot. Conditions are those of Figs. 1 and 2.

However, the OH sensitivity analysis for the sample case (Fig. 2) suggests that Rxn. 1 does not have a dominant role in controlling OH concentrations. The dilemma can be dismissed because the effects of Rxn. 1 are practically limited to a narrow time window when both reactants (CH_3 and HO_2) are near their peak concentrations, as evidenced by Fig. 2. As pointed out in Section 2.3, the strong temporal localization of the effect of Rxn. 1 can be attributed to the compounding effects of rapid rises and decays in CH_3 and HO_2 concentrations. In addition, the uncertainties in k_3, k_4 and k_5 have been minimized (Section 3.2) to further improve the accuracy in k_1 determinations.

A best-fit to the sample OH time-history yields $k_1 = 5 \times 10^{12}$ cm^3 mol^{-1} s^{-1}, as illustrated in Fig. 3. Comparing to the best-fit curve, an increase in k_1 can significantly boost OH concentration within a narrow time window as anticipated. A factor of 1.3 uncertainty in k_1 is estimated to be associated with the fitting process. At the first glance, the OH sensitivity analysis in Fig. 2 may suggest that strong interfering reactions, such as Rxns. 3–5, could introduce significant uncertainty in k_1. However, detailed examination reveals that the influences of interfering reactions are indeed significantly alleviated by the strong temporal localization of Rxn. 1 effects. When a 14% change in k_3 and the corresponding adjustment in k_5 are made simultaneously, k_1 needs to be varied by approximately 30% to re-match the experimental OH profile. k_3 and k_5 need to be adjusted concurrently to satisfy the constrain of initial OH concentrations, as has been demonstrated in the previous subsection. The 30% uncertainty inherited from the uncertainty in the k_3–k_5 pair also includes the counterpart that may stem from k_4 uncertainty, because Rxns. 3 and 4 have very similar OH sensitivities and are subject to same the constraint of initial OH concentrations. Therefore, a combined factor-of-1.4 uncertainty was estimated to be associated with k_1 values measured in this work.

3.4. Assessment of k_2

In contrast to Rxn. 1, which is able to significantly influence OH time-histories, Rxn. 2 does not do this (see Fig. 2) and therefore cannot be inferred from the OH time-history measurement. As discussed in Section 2.3, our choice was to investigate Rxn. 2 by studying time-histories of one of its reactants, HO_2. However, only the summation of k_1 and k_2 can be inferred from the HO_2 diagnostic because Rxns. 1 and 2 are nearly indistinguishable from the reactant side.

Figure 4 is an HO_2 sensitivity analysis for the sample case, where the HO_2 sensitivities to Rxns. 1 and 2 were combined. A strong negative sensitivity to "$CH_3 + HO_2 \rightarrow$ products" confirms the expectation that an increase in the summation of k_1 and k_2 can significantly reduce HO_2 concentrations in the reacting system. The best-fit to the 227 nm laser absorbance time-history was obtained by setting $k_2 = 3 \times 10^{12}$ cm^3 mol^{-1} s^{-1}, as demonstrated in Fig. 5. For comparison, k_1 and k_2 values were simultaneously adjusted by a factor of two and the resulting laser absorbance profiles were also plotted in the same figure.

Note that two major factors contribute to the evolution of 227 nm laser absorbance: the consumption of H_2O_2 and the growth and decline of HO_2. The portion of laser absorbance induced by H_2O_2 can be well-characterized because the evolution of H_2O_2 concentration is predominately controlled by Rxn. 3 (with a small uncertainty of ±14%) and is insensitive to the choices of k_1 and k_2

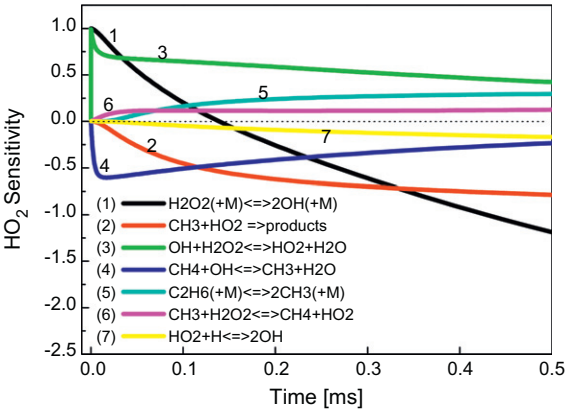

Fig. 4. HO_2 sensitivity plot of the conditions of Figs. 1–3.

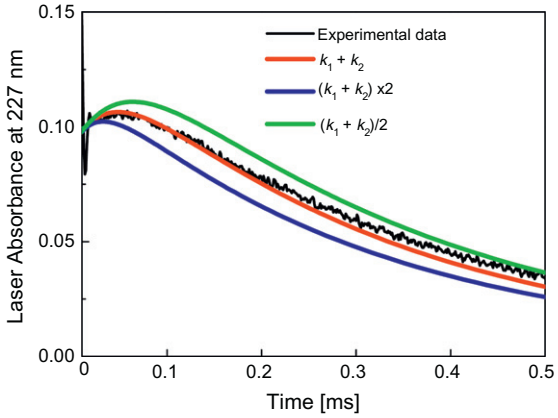

Fig. 5. A 227 nm laser absorbance time-history recorded within the same test where H_2O and OH time-histories presented in Figs. 1 and 3 were obtained. The laser absorbance time-history can be best fitted by setting $k_2 = 3 \times 10^{12}$ cm^3 mol^{-1} s^{-1}. Comparison with calculated total laser absorbance profiles with simultaneously doubled or halved k_1 and k_2 values are shown in the plot.

values. In addition, at temperatures near 1100 K, the H_2O_2 absorption cross-section at 227 nm is approximately one-tenth of that of HO_2 (1.4×10^5 cm^2/mol vs. 13.1×10^5 cm^2/mol) [16]. Therefore, changes in k_1 and k_2 values affect predictions of total laser absorbance at 227 nm through changes in calculated HO_2 time-histories, allowing the determination of $(k_1 + k_2)$ from the measurements of laser absorbance at 227 nm.

The fitting procedure introduces a factor of approximately 1.6 uncertainty in k_2, which also includes the uncertainties that stem from the uncertainties in the absorption cross-sections of H_2O_2 and HO_2. Interference reactions are responsible for additional uncertainty in k_2. The most direct competition with Rxn. 2 is Rxn. 1, which introduces a factor of 1.7 uncertainty in k_2. Three other major interfering reactions are C_2H_6 (+M) → $2CH_3$ (+M), $CH_3 + H_2O_2 \rightarrow CH_4 + HO_2$, and $HO_2 + H \rightarrow 2OH$. Using the uncertainty limits assigned to these reactions by the Baulch et al. review [6], k_2 uncertainty due to interfering reactions (excluding Rxn. 1) is estimated to be ±35%. Therefore, we may assume that k_2 can be determined to within a factor of 2.1 uncertainty.

3.5. Comparisons with previous studies

Experimentally determined k_1 and k_2 values from this work are summarized in Fig. 6 and Table 1. Between 1054 and 1249 K, no strong temperature dependence was observed for k_1 or k_2. The mean values are 6.8×10^{12} cm^3 mol^{-1} s^{-1} and 4.4×10^{12} cm^3 mol^{-1} s^{-1}

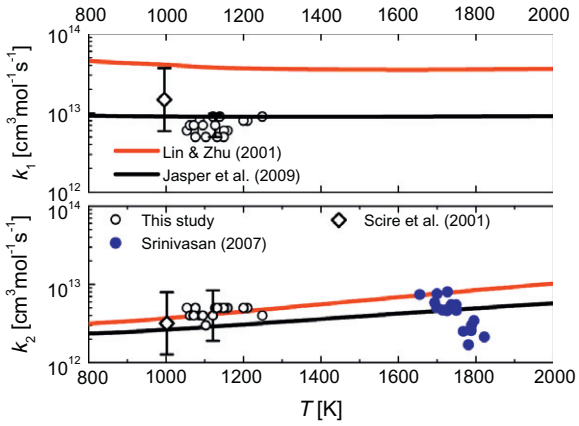

Fig. 6. (Upper): good agreement between the k_1 determinations of this work and the theoretical predictions by Jasper et al. [2] was found. (Lower): k_2 evaluations of this work agree very well with the Jasper et al. [2] and Lin and Zhu [4] predictions and the early experimental results reported by Srinivasan et al. [5].

for k_1 and k_2, respectively. Shown in the same plot are the results of two theoretical studies, with the k_1 prediction from Lin and Zhu [4] approximately 4.3 times that of Jasper et al. [2]. The large discrepancy between these two theoretical studies is echoed by similarly large discrepancies among k_1 expressions used by combustion mechanisms. For example, GRI-Mech 3.0 [10] uses $k_1 = 3.8 \times 10^{13}$ cm^3 mol^{-1} s^{-1}, whereas recent combustion mechanisms has set $k_1 = 0.9 \times 10^{13}$ cm^3 mol^{-1} s^{-1} (at 1000 K) [14] or 1.8×10^{13} cm^3 mol^{-1} s^{-1} [11].

It was previously recommended in the experimental studies by Scire et al. [8,9] to use lower k_1 values, where the authors perturbed the combustion of lean moist CO with CH_4. Although the agreement between the Scire et al. studies and the theoretical calculation by Jasper et al. is good, some uncertainty remains due to the indirect nature of the Scire et al. studies. As evidenced in Fig. 6, the measured k_1 values of this work are in excellent agreement with those of Jasper et al. With the small experimental uncertainty (a factor of 1.4), this work confirms that k_1 was over-estimated in the earlier studies [4,10].

Compared to k_1, k_2 is much less controversial. The calculated values from both theoretical studies agree well with each other, as demonstrated in Fig. 6. In addition, the results of this work are in excellent agreement with those of two previous experimental studies [5,8]. The good agreement implies that a higher value should be assigned to k_2 than estimates in early combustion mechanisms; GRI-Mech 3.0 sets $k_2 = 1.0 \times 10^{12}$ cm^3 mol^{-1} s^{-1} for instance.

Both theoretical studies [2,4] suggest very weak temperature dependency of k_1 and k_2. However, given the experimental uncertainties, the temperature range covered in this study (1054–1249 K) is not sufficiently wide to provide accurate information on temperature dependency of k_1 and k_2. The lower temperature limit was set by the detection limits of trace species, as OH and HO_2 concentrations became too low for current diagnostics. In addition, test times available for reflected shock wave experiments also set the low temperature limit. On the other hand, the time constants of target reactions become too short if temperature is too high. Experimental determination of k_1 and k_2 at other temperatures are needed to fully resolve these temperature dependencies.

A key parameter that is a direct derivative of k_1 and k_2 determinations is the branching ratio between Rxns. 1 and 2, which could be important in modeling high-pressure ignitions. Earlier combustion mechanisms use very large branching ratios; for example, the branching ratio adopted by GRI-Mech 3.0 is 38:1. Zhu and Lin [4]

Table 1
List of test conditions and results.

T_5 (K)	P_5 (atm)	$X_{H_2O_2}$ (ppm)	X_{CH_4} (ppm)	k_1 ($cm^3\ mol^{-1}\ s^{-1}$)	k_2 ($cm^3\ mol^{-1}\ s^{-1}$)	k_3 ($cm^3\ mol^{-1}\ s^{-1}$)	k_5 ($cm^3\ mol^{-1}\ s^{-1}$)
1139	3.679	1200	9943	9×10^{12}	5×10^{12}	7.65×10^{7}	1.73×10^{12}
1103	3.556	1240	9975	5×10^{12}	3×10^{12}	4.23×10^{7}	1.67×10^{12}
1121	3.494	1400	9961	9×10^{12}	5×10^{12}	5.71×10^{7}	1.65×10^{12}
1159	3.517	1540	9961	6×10^{12}	5×10^{12}	1.05×10^{8}	1.93×10^{12}
1072	3.584	1432	9958	6×10^{12}	4×10^{12}	2.46×10^{7}	1.53×10^{12}
1054	3.622	655	9982	6×10^{12}	5×10^{12}	1.96×10^{7}	1.45×10^{12}
1062	3.629	1260	9969	7×10^{12}	4×10^{12}	2.05×10^{7}	1.38×10^{12}
1127	3.449	1440	9975	7×10^{12}	5×10^{12}	5.47×10^{7}	1.74×10^{12}
1150	3.356	1420	9961	6×10^{12}	5×10^{12}	8.43×10^{7}	2.09×10^{12}
1249	3.259	1560	9973	9×10^{12}	4×10^{12}	3.80×10^{8}	2.20×10^{12}
1210	3.256	1887	9966	8×10^{12}	5×10^{12}	2.22×10^{8}	2.18×10^{12}
1200	3.379	1878	9966	8×10^{12}	5×10^{12}	1.88×10^{8}	1.89×10^{12}
1149	3.464	1490	9970	5×10^{12}	5×10^{12}	8.96×10^{7}	1.50×10^{12}
1132	3.543	1820	9924	5×10^{12}	5×10^{12}	6.83×10^{7}	1.60×10^{12}
1087	3.631	1290	9972	8×10^{12}	4×10^{12}	2.66×10^{7}	1.28×10^{12}
1095	3.628	1590	9959	7×10^{12}	4×10^{12}	3.82×10^{7}	1.43×10^{12}
1076	3.687	1661	9974	5×10^{12}	5×10^{12}	2.90×10^{7}	1.36×10^{12}
1072	3.772	1580	9972	7×10^{12}	4×10^{12}	2.46×10^{7}	1.34×10^{12}

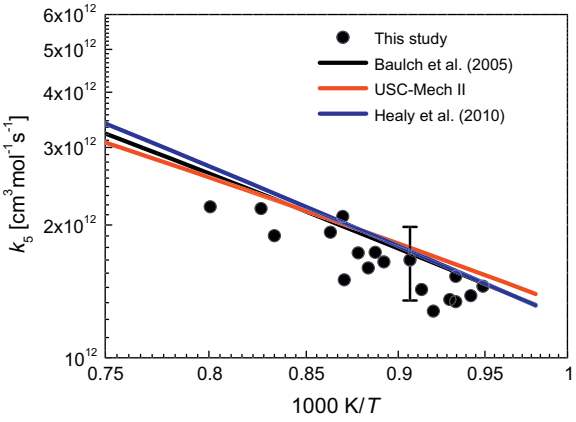

Fig. 7. The rate constants of reaction OH + CH_4 → H_2O + CH_3 (k_5) determined in this work compare favorably with previous recommendations [6,13,14].

predicted a branching ratio of 10:1 at 1000 K. A significantly reduced branching ratio (3:1) was recommended by Jasper et al. [2], which was subsequently adopted in a recent combustion mechanism [14]. With a branching ratio of 1.5:1, the current study supports the recent trend of using smaller branching ratios between Rxns. 1 and 2 in combustion mechanisms.

Although the primary targets of this work are k_1 and k_2, it is worth noting that k_3 and k_5 determinations compare favorably with previous recommendations. For example, the k_5 expression recommended by Baulch et al. [6] and the one adopted in USC-Mech II [13] (the base mechanism of this work) are both within the experimental uncertainty of the experimentally determined values, as evidenced by Fig. 7. In addition, the agreement between k_3 determinations of this study and those recently reported in literature [15–17] is excellent, with discrepancies well within the assigned experimental uncertainties. Given the similarity in experimental techniques used in this work and in previous studies, the determination of k_3 is not discussed further in this article.

4. Conclusions

CH_3 and HO_2 reactions were studied behind reflected shock waves between 1054 and 1249 K and near 3.5 atm using H_2O_2/CH_4/Ar blends as test mixtures. Reactions were initiated as H_2O_2 decomposed into OH radicals, which in turn reacted with H_2O_2 and CH_4 to produce a pool of HO_2 and CH_3 radicals. Using laser absorption spectroscopy, species time-histories of H_2O, OH and HO_2 were simultaneously measured behind reflected shock waves. Predictions of CH_4 ignition delays under high-pressure, intermediate-temperature conditions are very sensitive to the choice of the rate constant of reaction $CH_3 + HO_2 \rightarrow CH_3O + OH$ (k_1) in a combustion mechanism, because the reaction is a major chain-branching reaction. This paper reports the first experimental investigation of k_1, which was found to be 6.8×10^{12} $cm^3\ mol^{-1}\ s^{-1}$ with an estimated uncertainty factor of 1.4. The experimentally determined k_1 value of this work is in excellent agreement with the theoretical predictions reported by Jasper et al. [2] and is much smaller than the values used in some earlier combustion mechanisms, e.g., in GRI-Mech 3.0 [10].

The other major product channel for CH_3 and HO_2 reactions, $CH_3 + HO_2 \rightarrow CH_4 + O_2$ (Rxn. 2), is a chain-termination reaction. The rate constant (k_2) was experimental evaluated to be 4.4×10^{12} $cm^3\ mol^{-1}\ s^{-1}$, with an estimated uncertainty factor 2.1. The agreement with a previous experimental k_{-2} determination reported by Srinivasan et al. [5] and theoretical calculations [2,4] is remarkable, suggesting k_2 may be underestimated in earlier combustion mechanisms (e.g., GRI-Mech 3.0 uses $k_2 = 1.0 \times 10^{12}$ $cm^3\ mol^{-1}\ s^{-1}$). In addition, the rate constants of another major reaction of the reacting system, OH + CH_4 → CH_3O + OH, k_5, were found to be in excellent agreement with currently recommended values [6,13,14].

Acknowledgments

This work was supported by the National Science Foundation under Award No. 0649936, and the Department of Energy (National Nuclear Security Administration) under Award No. NA28614.

References

[1] E.L. Petersen, D.F. Davidson, R.K. Hanson, Combust. Flame 117 (1999) 272–290.
[2] A.W. Jasper, S.J. Klippenstein, L.B. Harding, Proc. Combust. Inst. 32 (2009) 279–286.
[3] E.L. Petersen, M. Röhrig, D.F. Davidson, R.K. Hanson, C.T. Bowman, Proc. Combust. Inst. 26 (1996) 799–806.
[4] R. Zhu, M.C. Lin, J. Phys. Chem. A 105 (2001) 6243–6248.
[5] N.K. Srinivasan, J.V. Michael, L.B. Harding, S.J. Klippenstein, Combust. Flame 149 (2007) 104–111.
[6] D.L. Baulch, C.T. Bowman, C.J. Cobos, et al., J. Phys. Chem. Ref. Data 34 (2005) 757–1397.
[7] M.B. Colket III, D.W. Naegeli, I. Glassman, Proc. Combust. Inst. 16 (1977) 1023–1039.
[8] J.J. Scire Jr., R.A. Yetter, F.L. Dryer, Int. J. Chem. Kinet. 33 (2001) 75–100.

[9] J.J. Scire Jr., F.L. Dryer, R.A. Yetter, Int. J. Chem. Kinet. 33 (2001) 784–802.
[10] G.P. Smith, D.M. Golden, M. Frenklach, et al., GRI-Mech, version 3.0, 2000. <http://www.me.berkeley.edu/gri-mech/>.
[11] A.A. Konnov, Detailed Reaction Mechanism for Small Hydrocarbons Combustion, release 0.5, 2007. <http://homepages.vub.ac.be/~akonnov/>.
[12] K.J. Hughes, T. Turanyi, M.J. Pilling, Leeds Methane Oxidation Mechanism, version 1.5, 2001. <http://garfield.chem.elte.hu/Combustion/Combustion.html>.
[13] H. Wang, X. You, A.V. Joshi, S.G. Davis, A. Laskin, F. Egolfopoulos, C.K. Law, USC Mech Version II. High-Temperature Combustion Reaction Model of H_2/CO/C1–C4 Compounds, 2007. <http://ignis.usc.edu/USC_Mech_II.htm>.
[14] D. Healy, N.S. Donato, C.J. Aul, E.L. Petersen, C.M. Zinner, G. Bourque, H.J. Curran, Combust. Flame 157 (2010) 1526–1539.
[15] Z. Hong, A. Farooq, E.A. Barbour, D.F. Davidson, R.K. Hanson, J. Phys. Chem. A 113 (2009) 12919–12925.
[16] Z. Hong, R.D. Cook, D.F. Davidson, R.K. Hanson, J. Phys. Chem. A 113 (2010) 5718–5727.
[17] Z. Hong, K.-Y. Lam, R. Sur, S. Wang, D.F. Davidson, R.K. Hanson, Accepted for oral presentation at the 34th International Symposium on Combustion.
[18] M.A. Oehlschlaeger, D.F. Davidson, R.K. Hanson, J. Quant. Spectrosc. Radiat. Transfer 92 (2005) 393–402.
[19] P. Zalicki, Y. Ma, R.N. Zare, E.H. Wahl, J.R. Dadamio, T.G. Owano, C.H. Kruger, Chem. Phys. Lett. 234 (1995) 269–274.
[20] K. Glänzer, M. Quack, J. Troe, Proc. Combust. Inst. 16 (1976) 948–960.
[21] J. Troe, Ber. Bunsen. Phys. Chem. 73 (1969) 946–952.
[22] H. Kijewski, J. Troe, Helv. Chim. Acta 55 (1972) 205–213.
[23] H. Hippler, J. Troe, J. Willner, J. Chem. Phys. 93 (1990) 1755–1760.
[24] M.A. Oehlschlaeger, D.F. Davidson, R.K. Hanson, Proc. Combust. Inst. 30 (2005) 1119–1127.
[25] A. E. Lutz, R.J. Kee, J.A. Miller, Senkin: A FORTRAN Program for Predicting Homogeneous Gas Phase Chemical Kinetics with Sensitivity Analysis, Report No. SAND87-8248, Sandia National Laboratory, 1988.
[26] Z. Hong, D.F. Davidson, E.A. Barbour, R.K. Hanson, Proc. Combust. Inst. 33 (2011) 309–316.